ACI MATERIALS JOURNAL TECHNICAL PAPER

Title no. 89-M49

Rate Effects and Load Relaxation in Static Fracture of Concrete

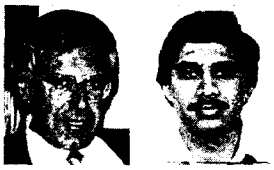

by Zdeněk P. Bažant and Ravindra Gettu

Reports an experimental study of the fracture of concrete at various crack mouth opening displacement (CMOD) rates with time to peak loads ranging from about 1 sec to 3 days (over five orders of magnitude). Tests were conducted on three-point bend specimens of three sizes in the ratio 1:2:4. Quasi-elastic fracture analysis, based on the effective modulus from creep theory, is used to evaluate the results according to the size effect method. The fracture toughness is found to decrease in agreement with the trend known for the dynamic range. The effective length of the fracture process zone is found to decrease with increasing rate, which implies increasing brittleness and a shift toward linear elastic fracture mechanics behavior for slow loading. Load relaxation at constant CMOD in the prepeak and post-peak stages of fracture tests was also investigated. The response tends to a straight line in the logarithm of elapsed time, and the post-peak relaxation is nearly twice as strong as the linear viscoelastic relaxation of unnotched specimens. The difference between these two relaxations must be caused by time-dependent processes in the fracture zone. The results reveal that in concrete there is a strong interaction between fracture and creep, which might cause the load-carrying capacity of structures with cracks to decrease significantly with load duration. However, extrapolations to loads beyond several days of duration would be speculative.

Keywords: beams (supports); **concretes; cracking (fracturing);** creep properties; **loads (forces); relaxation (mechanics).**

In all materials, even those that do not exhibit significant creep, fracture is rate-sensitive. That is, the effective fracture properties depend on the crack growth rate, which is determined by the loading rate. This is due to the fact that the rupture of interatomic or intermolecular bonds is a thermally activated process. The probability that the thermal vibration energy of an atom or molecule (depending on the load) would exceed the activation energy barrier of the bond increases with the number of oscillations. It is (according to the Maxwell distribution of thermal energies) equal to zero for an infinitely short time interval. In a material such as concrete, the rate sensitivity is expected to be particularly marked due to creep of the material in the fracture process zone, as well as in the entire structure. Studies by Shah and Chandra,[1] Wittmann and Zaitsev,[2] Liu et al.,[3] and others have suggested that fracture is affected by creep. Yet a detailed investigation of this effect has not been conducted. Substantial studies (Mindess and Shah[4]) have been carried out under very high (dynamic) rates of loading, in which the maximum load is reached under 1 s. Since the creep effect in this range is weak, a comprehensive understanding of rate effects can be obtained without accounting for creep. However, for slower rates, the contribution of creep becomes significant. Fracture, with rates that correspond to reaching maximum load within anywhere between an hour and several years, is of great interest for predicting the long-term cracking and failure of many types of concrete structures. For example, as is now widely accepted, the failure of dams should be analyzed according to fracture mechanics, but certain types of fracture in dams develop gradually over a period of many years. Without any test data, one cannot but speculate about the effective fracture properties to be used under such slow rates.

This paper presents the results of fracture tests of concrete at various loading rates in the static range, with the time to peak load ranging from 1 s to 2.5 days, and the results of complementary tests of load relaxation in fracture specimens. (A preliminary report was made earlier at two conferences.[5,6]) The size effect method, combined with the assumption of a quasi-elastic effective modulus representation of concrete creep, is used to determine the fracture energy, fracture toughness, effective length of the process zone, and effective crack-tip opening displacement at various loading rates.

REVIEW OF RATE PROCESSES IN CONCRETE FRACTURE

The significance of rate effects may be illustrated by comparing the results of two tests on identical three-

ACI Materials Journal, V. 89, No. 5, September-October 1992.
Received June 25, 1991, and reviewed under Institute publication policies.

Zdeněk P. Bažant, FACI, holds the W. P. Murphy professional chair at Northwestern University, Evanston, Ill., where he served as Director of Center for Concrete and Geomaterials (a predecessor to the current Center for Advanced Cement-Based Materials). Dr. Bažant, a registered structural engineer, has served as consultant to Argonne National Laboratory and other firms; is Editor (in chief) of the ASCE Journal of Engineering Mechanics; *President of the newly formed International Association for Fracture Mechanics of Concrete Structures (FraMCoS); Chairman of ACI Committee 446, Fracture Mechanics, RILEM creep committee, ASCE-EMD Programs Committee, and SMiRT's Division H; and is on the Board of Directors of the Society of Engineering Science. He has received numerous awards, the latest of which is the 1990 Gold Medal from the Building Research Institute of Spain, and an honorary doctorate from Czech Technical University at Prague.*

ACI member **Ravindra Gettu** *is a Senior Researcher in Construction Engineering at the Technical University of Catalunya, Barcelona, Spain. He has a PhD from Northwestern University and a BEngng from the University of Madras, India. He is a member of ACI Committee 446, Fracture Mechanics. His current research interests include the behavior and modeling of structural materials, fracture mechanics, and high-strength concrete.*

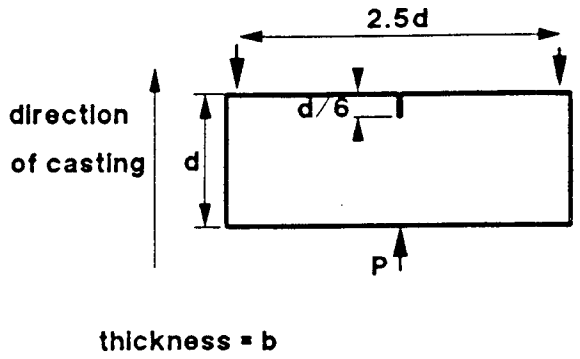

Fig. 1 — Three-point bend fracture specimen

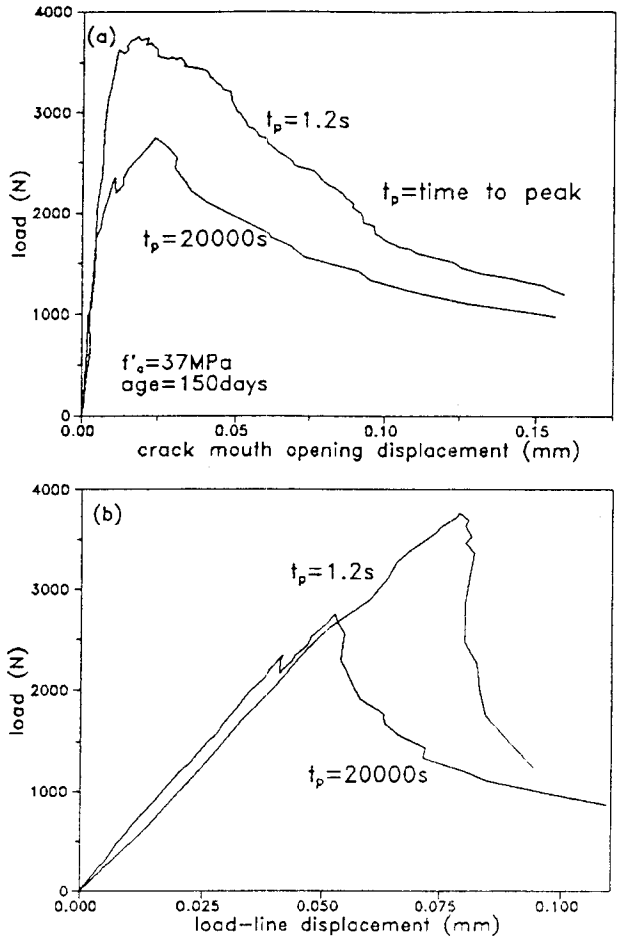

Fig. 2 — Rate effects on (a) load-CMOD response and (b) load-deflection response

point bend (3PB) fracture specimens (see Fig. 1: b = 38 mm, d = 76 mm, f'_c = 37 MPa, age = 150 days), at very different crack mouth opening displacement (CMOD) rates. The peak load of one specimen was reached in 1.2 s, and that of the other in about 20,000 s (5.6 hr). The load versus CMOD and load-versus-load-line displacement curves are shown in Fig. 2(a) and (b). The peak load of the faster test is more than 25 percent higher than that of the slower test. A similar increase in the failure stress or "strength" has been observed previously in the static range by several investigators.[7] A similar trend exists under dynamic or impact loading.[8,9]

Comparison of the post-peak response is also very interesting. While the load-CMOD plots [Fig. 2(a)] for both specimens are quite similar, the load-displacement plots [Fig. 2(b)] differ significantly. For the faster test, the load-displacement curve descends steeply, whereas in the slower test the drop is gradual and closer to ductile behavior. This difference can be attributed to creep in the bulk of the specimen, since the load-line displacement reflects the cumulative response of the entire specimen, whereas CMOD is affected primarily by the deformations of the crack and the fracture process zone. It is therefore important that the effect of creep outside the process zone be separated from the rate process producing fracture. It also appears that CMOD-controlled tests are more relevant for studying fracture properties than deflection-controlled tests.

It has been suggested that the cause for the increase in concrete strength under fast loading is the change in crack path with rate. At very high (dynamic) loading rates, it has been observed (e.g., from compressive impact tests of Hughes and Watson[10]) that cracks tend to be less tortuous, and often pass through the aggregates instead of following the aggregate-mortar interfaces. Since aggregates, in normal concrete, are stronger than both the mortar and the interfaces, a crack passing through the aggregates will encounter a higher resistance than one following the interfaces. To investigate whether this change in mechanism occurs in the static regime, the fractured surfaces of two 3PB specimens (see Fig. 1: b = 38 mm, d = 76 mm, age = 45 days) — one with time to peak load t_p = 0.5 s (and peak load = 4000 N), and the other with t_p = 30,000 s (and peak load = 2340 N) — were studied. It can be seen, from Fig. 3, that a few more aggregates were fractured in the faster case than in the slower, but no significant change in the fracture mechanism is apparent.

The straightening of the crack path could also have an opposite effect — strength decrease due to the higher stress intensity of planar cracks. Crack bridging and deflection by the aggregates increase the overall fracture resistance. To check for difference in tortuos-

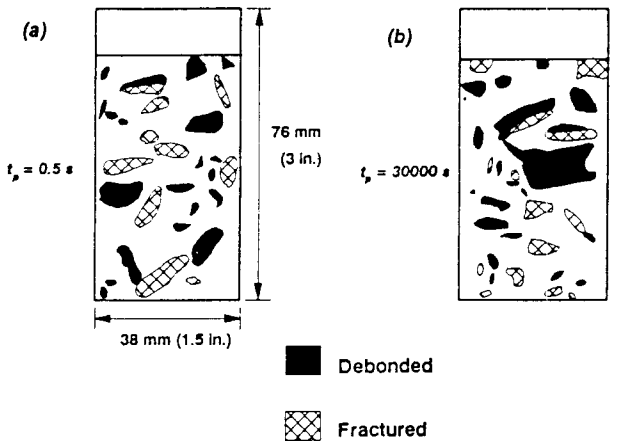

Fig. 3 — Crack surfaces for (a) t_p = 0.5 s and (b) t_p = 30,000 s

ity, the fractured areas of the specimens mentioned previously were approximately determined. After complete fracture, the cracked surfaces were covered with 2.4-mm (0.094-in.) wide tape, and the crack area was calculated from the length of the tape used. Although this method is not very accurate, it seems to suffice for the present purpose. The crack area for the faster fracture was 2900 mm² (4.5 in.²) and for the slower one, 3000 mm² (4.7 in.²). (The crack-plane areas were 2420 mm² (3.75 in.²) for both.) This difference is insignificant. Therefore, it seems that the same mechanisms dominate fracture in this range. (A similar observation was made from tests of certain ceramics by Suresh et al.[11]; they showed that fracture initiation in alumina was predominantly intergranular for both dynamic and static rates.)

Several micromechanical processes could give rise to rate effects, as, for example, the presence of moisture at the crack tip. As is well known, wet surfaces require less energy to form than dry surfaces, i.e., the fracture energy decreases in the presence of moisture. Water corrosion and disjoining pressure mechanisms that weaken the bonds at the fracture front may also be involved.[12] Such effects could explain the lowering of fracture energy and strength in rock[13] and concrete.[14] The detrimental effect of moisture is more significant at slower rates and tends to increase the crack velocity. It has even been suggested that the water in concrete is the primary source of rate effects.[9,15]

Creep dominates the response of cracked as well as uncracked concrete under slow and sustained loading. It may considerably decrease the strength and the effective modulus as loading rate becomes slower. The effects of creep on fracture, however, may be complicated.[12] One effect may be a decrease in fracture resistance, and another effect may be relaxation at the crack tip, which removes part of the stress concentration. However, the second effect would also reduce the extent of microcrack initiation ahead of a propagating crack.[16,17] Since the microcracked zone causes crack blunting or toughening, a smaller zone implies more brittle fracture.

Table 1 — Fracture test data

Series	Specimen depth, mm	CMOD rate, mm/s	Time to peak t_p, sec	Age at loading, days	Peak load, N
Fast	38	1.1×10^{-2}	0.9	28	2225
		8.4×10^{-3}	2.2	28	1800
f'_c = 36.6 MPa		1.1×10^{-2}	1.5	28	1890
ω = 1.3 percent	76	1.4×10^{-2}	1.3	28	3625
		1.4×10^{-2}	2.2	28	3960
		1.4×10^{-2}	1.3	28	3025
	152	2.1×10^{-2}	1.3	28	6180
		2.1×10^{-2}	1.1	28	5940
		2.1×10^{-2}	1.1	28	5425
Usual	38	1.8×10^{-5}	595	28	1825
		1.8×10^{-5}	595	28	1780
f'_c = 36.5 MPa		2.4×10^{-5}	570	28	1645
ω = 6.1 percent	76	5.3×10^{-5}	460	28	3070
		3.6×10^{-5}	520	28	2800
		4.3×10^{-5}	505	28	2760
	152	7.1×10^{-5}	495	28	5025
		7.1×10^{-5}	360	28	4225
		7.1×10^{-5}	420	28	4200
Slow	38	7.1×10^{-7}	10,350	40	2315
		7.1×10^{-7}	17,100	38	1935
f'_c = 37.2 MPa		7.1×10^{-7}	13,500	39	2180
ω = 5.5 percent	76	1.0×10^{-6}	10,625	46	3580
		9.4×10^{-7}	17,550	42	3515
		1.1×10^{-6}	11,900	30	3180
	152	1.4×10^{-6}	15,300	32	4270
		1.4×10^{-6}	14,850	38	4180
		1.7×10^{-6}	14,600	31	5295
Very slow	38	3.8×10^{-8}	266,500	120	2135
f'_c = 36.9 MPa	76	7.4×10^{-8}	255,500	108	3180
ω = 4.4 percent	152	1.3×10^{-7}	236,000	90	4580

f'_c = 28-day compressive strength of 76 × 152-mm cylinders.
ω = coefficient of variation of f'_c.
1 MPa = 145.04 psi; 1 N = 0.2248 lb.

Even at dynamic strain rates, it is not clear whether a slower rate causes more or less brittleness. Assuming the behavior to be analogous to that of a plastic material with coalescing voids, Reinhardt[18] proposed that when the crack velocity is comparable in magnitude to the wave speed near the crack tip, the fracture process zone becomes larger than usual. To a certain extent, this hypothesis is supported by tests. Impact tests show more distributed cracking and more fragmentation at higher strain rates.[9,19] These results further imply that faster fracture is more ductile, since it dissipates more energy in a larger zone.[20] On the other hand, since the nonlinearity of the prepeak load-deformation relationship decreases with an increase in loading rate, several investigators have argued that fracture becomes more brittle.[21] That argument applies only when the nonlinearity is primarily due to the fracture process, and the effects of time-dependent phenomena outside the fracture zone are negligible. It is also possible that different trends could exist due to a change in fracture mechanisms, for example, fracture through or around aggregates and inertia effects. Reversals suggesting such explanations have been documented for failure strain[12] and fracture parameters.[22] The present study is limited to static rates, and, therefore, will not attempt to answer these questions for fracture in the dynamic range.

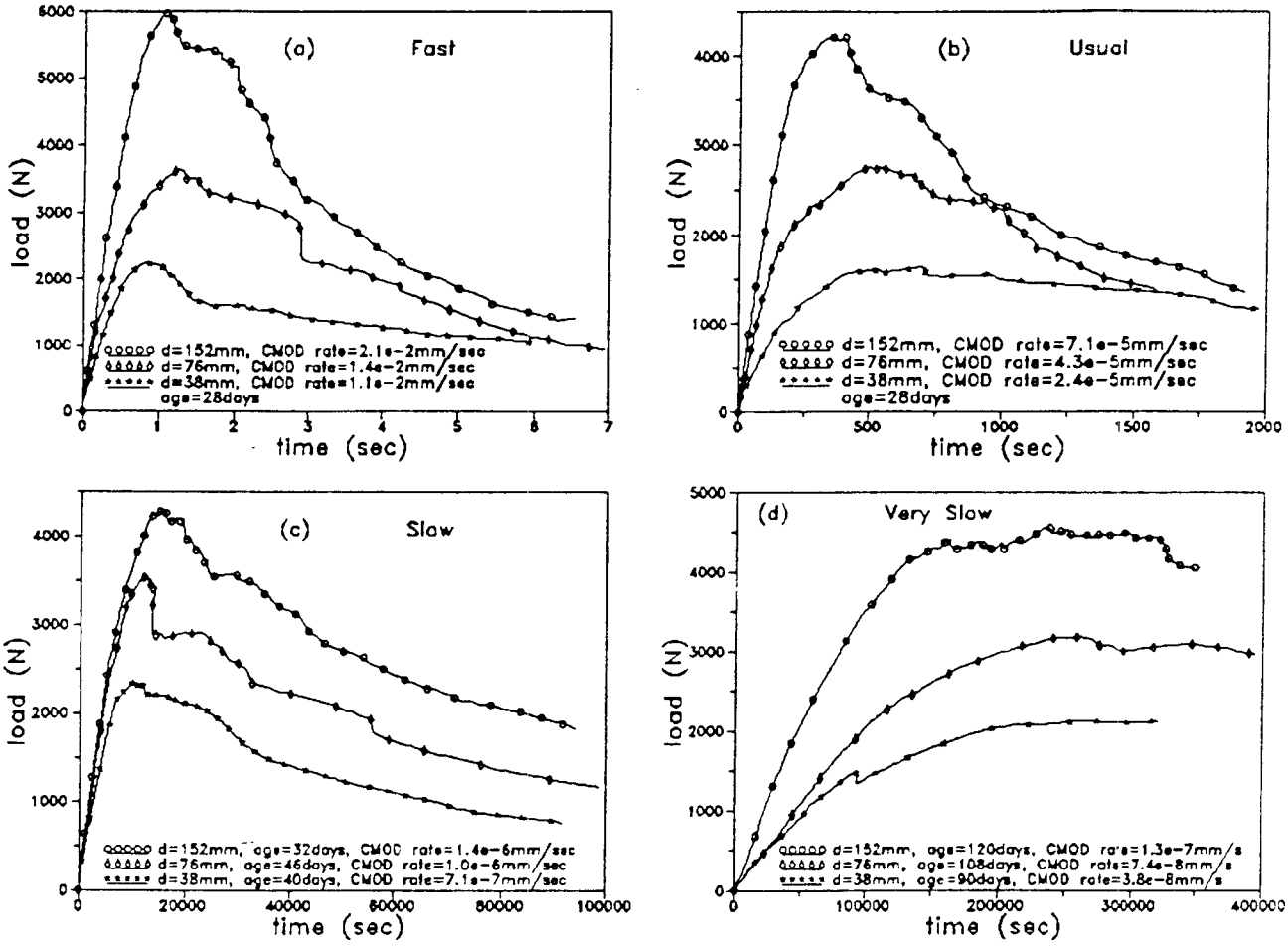

Fig. 4 — Typical load-CMOD curves (e − n means × 10^{-n})

TEST SPECIMENS

Three-point (single-edge notched) bending specimens (Fig. 1) were used with concrete of cement:sand: gravel:water ratio 1:2:2:0.6, Type I cement, crushed limestone gravel (maximum grain size = 13 mm), and standard No. 2 sand (maximum grain size = 5 mm). The beams were cast with the notch face at the bottom. The thickness of the specimens was 38 mm (1.5 in.), and the notch length was ⅙ of the beam depth. The notches, cut with a diamond band saw, were 1.8 mm (0.07 in.) wide. All the specimens were cured under water until testing, and had their surfaces sealed with siliconized acrylic latex during testing to prevent loss of moisture. The fracture tests were conducted under CMOD control in a 89-kN (20-kip) load frame with a load cell operating in the 8.9-kN (2000-lb) range. Companion cylinders of 76-mm (3-in.) diameter and 152-mm (6-in.) length were used to determine the compressive strength f'_c 28 days after casting. The cylinders were capped with a sulfur compound, and tested in a 534-kN (120-kip) load frame under stroke control such that failure occurred in about 10 min.

SIZE EFFECT TESTS AT VARIOUS CMOD RATES

Four series of tests, each with specimens that were geometrically similar in two dimensions and of three sizes [d = 38, 76, and 152 mm (1.5, 3, and 6 in.)], were conducted. The measured peak loads and other details are listed in Table 1. The typical measured load-CMOD curves are presented in Fig. 4. The CMOD rates were chosen to give almost the same t_p for all the sizes in each series (Table 1). The range of CMOD rates, or t_p, exceeds five orders of magnitude (1:10^5).

In choosing the loading rates at different sizes, one must realize that the same displacement rate used for specimens of different sizes will result in different rates of deformation of the fracture process zone. Assuming linear viscoelastic behavior through the whole volume of the specimen, one could calculate the load-point displacement rates that give the same rate $\dot{K}_I$ of the stress intensity factor K_I for specimens of different sizes (this is achieved for $dP/dt = \sqrt{d} \times const.$). But due to nonlinear behavior and the presence of a large fracture process zone, this does not achieve the same rates of deformation of the fracture process zone, which is the condition for which the results for large and small specimens can be legitimately compared. To calculate the CMOD rates that meet this condition, one would need a priori a good mathematical model for the rate effect in fracture. But such a model is unavailable. Among various simple possibilities, the condition of equal rates of deformation of the fracture process zone

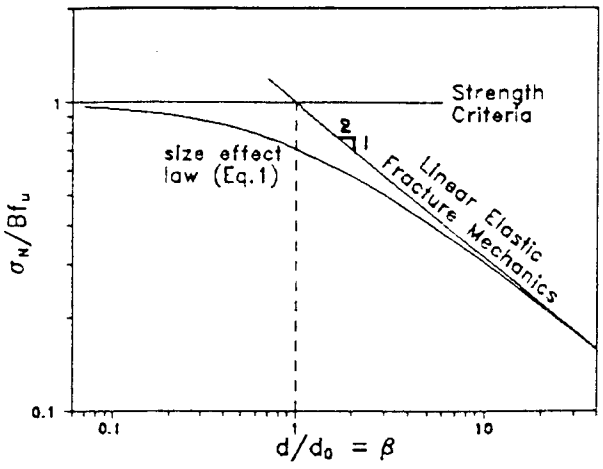

Fig. 5 — Size effect law

is probably best achieved by rates that give approximately the same time t_p to peak load. This conditon at the same time insures that the relative creep deformations outside the process zone at time t_p are about the same — another conditon desired for comparability of different sizes. The rates to achieve equal t_p were selected on the basis of prior experimentation, and the condition of equal t_p has of course been achieved only approximately. The corresponding CMOD rates for various specimen sizes were not equal, but they were of the same order of magnitude (Table 1). However, once the test results are translated into a mathematical model, the loading rate selection should in the future be done by calculations.

The purpose of using specimens of different sizes was to apply the size effect method for determining fracture parameters. The method is based on the size effect law,[23] which in its simplest form reads (Fig. 5)

$$\sigma_N = \frac{Bf_u}{\sqrt{1 + \beta}}, \beta = \frac{d}{d_0} \quad (1)$$

where $\sigma_N = P_u/bd$ = nominal strength (maximum nominal stress), P_u = peak (maximum) load, d = characteristic dimension of specimen (here, chosen as the specimen depth), b = thickness, β = brittleness number, Bf_u and d_0 are the parameters of the model, and f_u is some estimate of the material strength. When the size is very small, i.e., $\beta \ll 1$, σ_N is not significantly affected by size, and the behavior is then governed by strength limit (or allowable stress) criteria. This implies that energy is dissipated during failure in a relatively large region. When β is large, $\beta \gg 1$, the behavior follows linear elastic fracture mechanics (LEFM), and $\sigma_N \propto 1/\sqrt{d}$. In this case, energy is dissipated in a region of infinitesimal size at the crack tip. The transition zone (taken as $0.1 < \beta < 10$), in which the test results usually lie, is the nonlinear fracture regime.

Eq. (1) has been extensively verified for the fracture of concrete and extended to determine fracture parameters and material brittleness.[24,25] The method has also been used to determine the change in fracture properties with temperature[14] and strength.[26] However, all the tests have so far been conducted at conventional loading rates, i.e., with t_p between 5 and 10 min. Applicability of the method at various rates is to be experimentally validated. For Eq. (1) to apply, specimens of each size should attain the peak load in about the same time, for reasons already explained (differences up to 50 percent are probably not serious, but differences in orders of magnitude certainly would be). The reason is that, for all sizes, the fracture process zone should be deformed at about the same rate, and the relative creep deformations outside the process zone should be about the same.

To determine the size effect parameters in Eq. (1) from σ_N-data, this study used nonlinear regression analysis in which the sum of the squared errors in σ_N is minimized. The optimized values of Bf_u and d_0, obtained by means of the Marquardt-Levenberg algorithm (available in standard computer libraries), are listed in Table 2 for each series of tests. The curves in Fig. 6 are the optimum fits of the data points by Eq. (1). The coefficients of variation of the deviations of σ_N from the fits are also given. The results demonstrate that the size effect is significant at all the rates used, and that Eq. (1) fits the data reasonably well through the entire time range.

The applicability of Eq. (1) might be questioned, since its theoretical derivation assumes the behavior outside the process zone to be elastic. There are, nevertheless, two justifications: 1) according to the double power creep law,[27] the ratio of creep strain to the true instantaneous strain, at 28 days, is about 0.9 for t_p = 8 min (the usual static test), about 0.4 for t_p = 1 s, and about 1.9 for t_p = 2.5 days. If elastic analysis is acceptable for the ratio 0.9, it should also be acceptable in the range 0.4 through 1.9, provided, of course, the duration of the loading is the same for all the sizes; 2)

Table 2 — Material fracture parameters

Series	Average t_p, sec	Average age, days	Bf_u, MPa	d_0, MPa	ω	K_{Ic}, MPa$\sqrt{mm}$	c_f, mm	E_{eff}, GPa	G_f, N/m	δ_{ef}, mm
Fast	1.4	28	1.60	102.5	0.10	39.5	17.2	36.0	43.4	0.0146
Usual	500	28	1.68	41.3	0.06	26.3	6.9	28.6	24.1	0.0077
Slow	13,650	38	2.94	13.3	0.09	26.1	2.2	24.1	28.4	0.0052
Very slow	253,000	106	3.47	8.5	0.01	24.6	1.4	22.4	26.9	0.0042

ω = coefficient of variation of the deviations of the fit from test data.

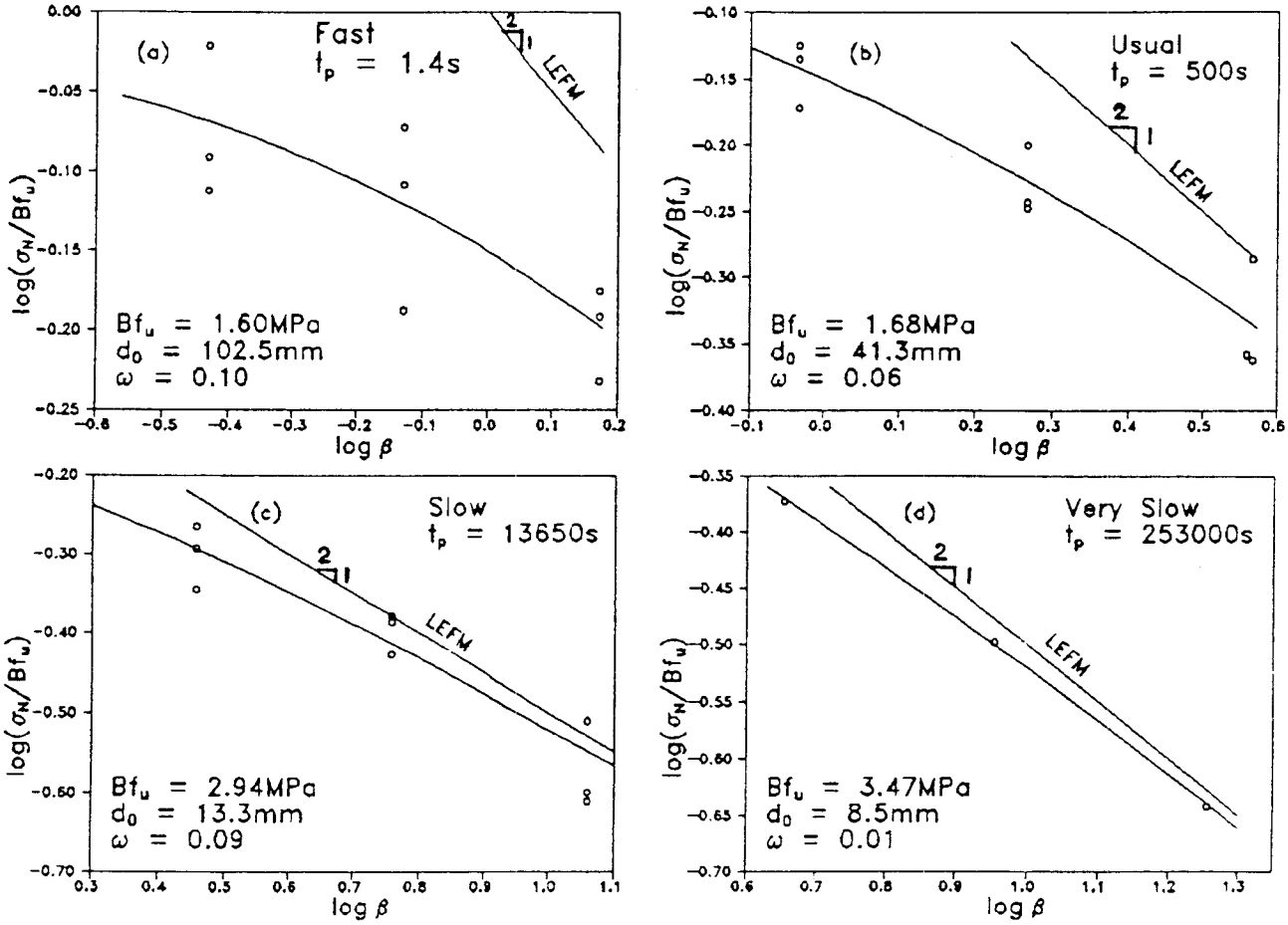

Fig. 6 — Optimum size effect curves for the test data

due to linearity of creep and the rapidly decaying nature of the creep curve of concrete (for stresses up to about half the strength), quasi-elastic analysis based on the effective modulus is a reasonable approximation to the viscoelastic solution.[27]

SHIFT IN BRITTLENESS

Since the test results for all the rates agree reasonably well with the size effect law, they can be combined into one plot, as in Fig. 7. Such a combined plot was used previously to show the increase in the brittleness of concrete with increasing strength.[26] This clarifies the effect of rate on the brittleness number. In each series there are three sets of data. In each set, the most brittle (largest β) are the largest specimens, and the least brittle are the smallest. Now, the interesting aspect is that there is a significant shift of the data sets toward the right (toward LEFM, i.e., ideal brittle failure) as t_p increases. This means that fracture becomes more brittle as the loading becomes slower; i.e., the intensity of the crack-tip shielding mechanism decreases as the loading rate becomes slower. The damage and energy dissipation are more distributed for higher rates. It should be emphasized, however, that even though the present quasi-elastic approximation approaches LEFM for very slow loading rates, consideration of creep in the analysis of structural response becomes more important.

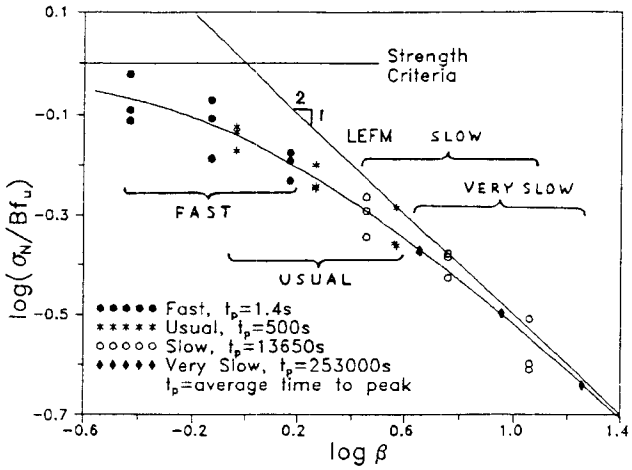

Fig. 7 — Change in mode of failure with loading rate

This result is similar to that of Bažant and Prat,[14] who applied the size effect method to tests of fracture specimens at different temperatures. From their data it can be seen that the brittleness of concrete increases with temperature. The effect of time on fracture is analogous to the effect of high temperature, since a higher temperature means higher creep. This similarity reinforces the present conclusion.

Another extrapolation of the effect of creep on brittleness could be made to the failure of early-strength concrete. Since creep mechanisms are more dominant at

Table 3 — Fracture parameters corrected for 28 days

Series	E_{eff}, GPa	K_{Ic}, MPa$\sqrt{mm}$	c_f, mm	G_f, N/m	δ_{ef}, mm
Fast	36.0	39.5	17.2	43.4	0.0146
Usual	28.6	26.3	6.9	24.1	0.0077
Slow	22.9	25.3	2.2	28.1	0.0052
Very slow	18.2	22.7	1.3	28.2	0.0047

younger ages, one could infer from this study that fracture is more brittle in concrete at earlier ages. The data of Wong and Miller[28] on fracture tests at different ages (t_p = 5 to 10 min) support this inference.

FRACTURE PARAMETERS OBTAINED BY THE SIZE EFFECT METHOD

The steepness of post-peak load-deflection curves, or the amount of distributed cracking in unnotched specimens, have previously been interpreted as indicators of material brittleness. Though valid in certain cases, such indicators are not size-independent and general measures. Rather, objective measures must be based on fracture mechanics. In the present study, the size of the fracture process zone is taken as the measure of brittleness; a material with a smaller process zone is more brittle. The structural brittleness, on the other hand, may be generally characterized by the brittleness number β = Eq. (1). Another important fracture parameter is the fracture toughness; higher fracture toughness implies higher resistance against failure. These quantities are also necessary for nonlinear fracture mechanics analysis of concrete structures.

Since specimen size and shape could have a strong effect on the measurements of fracture parameters, extrapolation to an infinitely large size has been proposed for obtaining unambiguous values.[29] It has also been shown that parameters obtained in this manner are practically independent of specimen geometry.[24] Based on the infinite size extrapolation of Eq. (1), simple expressions for fracture energy G_f, fracture toughness K_{Ic}, effective length of the fracture process zone c_f, and effective critical crack-tip opening displacement δ_{ef} have been derived[25,29,30] (see also RILEM recommendation[31])

$$G_f = \frac{1}{E'}(Bf_u)^2 d_0 g(\alpha_0) \quad (2)$$

$$K_{Ic} = Bf_u\sqrt{d_0 g(\alpha_0)} \quad (3)$$

$$c_f = \frac{d_0 g(\alpha_0)}{g'(\alpha_0)} \quad (4)$$

$$\delta_{ef} = \frac{8K_{Ic}}{E'}\sqrt{\frac{c_f}{2\pi}} \quad (5)$$

where function $g(\alpha)$ is the nondimensionalized energy release rate defined by the LEFM relation $G = P^2 g(\alpha)/E'b^2 d$, G = the actual energy release rate, P = load, α = (crack length)/d = relative crack length, $\alpha_0 = a_0/d$, a_0 = notch or traction-free crack length, $E' = E$ for plane stress, $E' = E/(1 - \nu^2)$ for plane strain, E = Young's modulus, ν = Poisson's ratio, and $g'(\alpha) = dg(\alpha)/d\alpha$. The function $g(\alpha)$ can be obtained from handbooks[32] or from LEFM analysis.

Parameter c_f lumps together the effect of all the toughening mechanisms in concrete, including the deflection and bridging of the crack by aggregates, and microcracking ahead of the crack tip. Note also that the crack tip is defined here as the point where the traction-free crack ends.

For the present specimen geometry, finite element analysis provided the values $g(\alpha_0) = 5.927$ and $g'(\alpha_0) = 35.24$. The values of Bf_u and d_0 obtained earlier (Table 2) can then be used in Eq. (3) and (4) to calculate K_{Ic} and c_f; see Table 2. (Note that the calculated values of K_{Ic} and c_f can have coefficients of variation up to 0.3 and 0.5, respectively.)

In view of the preceding comments, the validity of Eq. (2) through (5) may be extended to linear viscoelastic creep, which occurs in most of the specimens except in (and very near) the fracture process zone. This is done by replacing E with the effective modulus E_{eff} (inverse of the compliance function) corresponding to load duration t_p. To determine E_{eff} the BP model for the prediction of concrete creep[27,33] was used. Only the basic creep was considered, since the specimens were sealed to prevent moisture loss. In applying the BP model, the asymptotic modulus was modified such that the effective modulus for the loading time of 10 min would coincide with the ACI code formula $E = 4735\sqrt{f'_c}$, in MPa (or $E = 57{,}000\sqrt{f'_c}$, in psi). The E-values for the various test series are listed in Table 2. Using the effective moduli in Eq. (2) and (5), the values of G_f and δ_{ef} are computed and listed in Table 2.

Since two series of tests were conducted at ages other than the standard 28 days, the fracture parameters obtained from them should be corrected before comparisons are made. The following formulas were used for this purpose: $f'_t = 0.50\sqrt{f'_c}$ (ACI); $f'_c(t) = f'_c(28)\, t/(4 + 0.85t)$ (ACI); and $G_f \propto (2.72 + 3.103 f'_t)\, f'^2_t d_a/E_{eff}$ (Reference 34), where f'_t is the tensile strength; f'_c, f'_t, and E are in MPa; d_a is the maximum aggregate size in mm; G_f is in N/mm; t is the age in days; and E_{eff} is obtained from the BP model, as before. It was also assumed that the parameter Bf_u varies linearly with f'_t. (Possible errors in these formulas cannot be important, since the corrections are small.) The adjusted 28-day values of all the parameters are listed in Table 3.

DISCUSSION OF TRENDS OBSERVED IN CONSTANT-RATE TESTS

From Table 3, it is clear that the fracture toughness K_{Ic} tends to decrease with increase in t_p. This agrees with the well-known reduction in concrete strength as the loading rate becomes slower. The trend agrees with those obtained by other methods for mortar and cement paste.[35]

A new result from the present tests is the significant decrease in the fracture process zone c_f as the loading rates decrease. This implies that the material brittle-

ness, and consequently the brittleness of structural failure, increases due to creep. The decrease in c_f is probably due to the relaxation of the high stresses in the material ahead of the crack tip, causing the stress drop to be more concentrated. The trend can be approximately described by the formula [see Fig. 8(a)]

$$c_f = c_0 \left(\frac{t_0}{t_p}\right)^n \quad (6)$$

where t_0 is the reference value of time to peak and c_0 is the corresponding value of c_f; $n = 0.22$; and for $t_0 = 600$ s (about the conventional testing time), $c_0 = 5.04$ mm.

Along with K_{Ic} and c_f, δ_{ef} is found to also decrease for slower loading. This trend agrees with that observed by Wittmann et al.,[22] who, however, concluded that for very slow loading, the trend reverses. The trend may also be different in the dynamic range.[21]

The variation of the fracture toughness of mortar and cement paste with loading rate has been described by means of a power function[35] $K_{Ic} = K_0 v^m$, where K_0 and m are parameters determined experimentally, and v is the rate of change of deflection, crack length, or stress. Similarly, the present test results have been fitted [Fig. 8(b)] by the equation

$$K_{Ic} = K_0 \left(\frac{v}{v_0}\right)^m \quad (7)$$

where $v \cong \delta_{ef}/t_p$, v_0 is the chosen reference deformation rate, and $K_0 = K_{Ic}$ for $v = v_0$. From the present data, $m = 0.041$, and for $v_0 = 5 \times 10^{-5}$ mm/s, $K_0 = 30.4$ MPa$\sqrt{\text{mm}}$.

For loading rates faster than the usual static test, the fracture energy G_f has previously been found to increase significantly with an increase in rate.[8,36] However, at low rates, this trend is not obvious from the present results. This may be because G_f is strongly affected by the decrease in the effective modulus due to creep. Wittmann et al.[22] proposed that fracture energy increases under very slow loading due to the influence of creep. The present variation tends to agree with their conclusion, but the scatter of the present results for G_f is too high to draw a firm conclusion. If linear elastic fracture mechanics were applicable, then one could use the relation $G_f = K_{Ic}^2/E$ to determine that the scatter is due to E, but the relation of G_f and K_{Ic} is more complicated.

RELAXATION TESTS OF UNNOTCHED BEAMS

To determine the creep or relaxation behavior of the concrete used, four unnotched beams, with $b = 38$ mm (1.5 in.), $d = 76$ mm (3 in.), and span = 191 mm (7.5 in.), were tested under three-point loading. A transducer (LVDT of 0.127-mm range) fixed on the beams measured the deformation over a gage length of 25.4 mm (1 in.) centered along the tension face. A computer-based data acquisition system monitored the load and deformation. Test details are listed in Table 4. Using the beam theory, the maximum bending stress and strain were calculated as a function of time. The initial load P_1 was applied at a rate of maximum strain equal to 3.6×10^{-4}/s, which corresponds to the time to peak $t_p \cong 1$ s. After time t_1, at which the desired P_1 was reached, the deformation was held constant, and the specimen was allowed to relax the load. The tests were conducted with different P_1-values. The measured relaxation curves of maximum bending stress σ versus elapsed time $(t - t_1)$ are shown in Fig. 9(a). It so happened after that some time the tests could not be controlled, since the transducer started to slip; only the data for the duration of proper control are shown.

The relaxation is strongest in Specimen U4, which had the highest P_1-value. It appears that U4 is in the

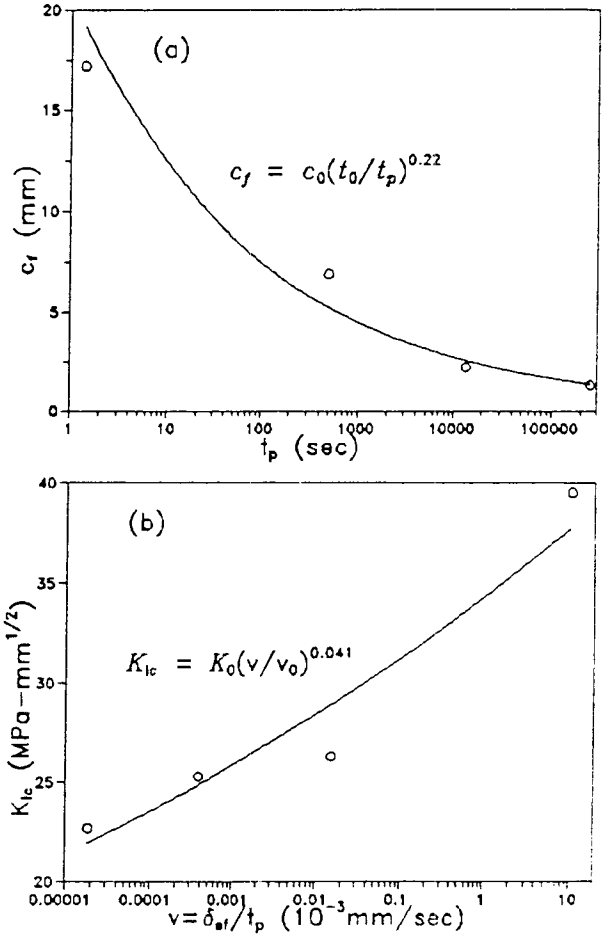

Fig. 8 — Effect of time to peak load on (a) fracture process zone size and (b) fracture toughness

Table 4 — Details of relaxation tests of unnotched beams

Specimen	Age, days	P_1, N
U1	34	990
U2	39	3420
U3	31	3760
U4	30	4580

P_1 = load at which relaxation started.
Approximate peak load = 5600 N at 35 days.
Strain rate during loading = 3.6×10^{-4}/sec.
f'_c = 28.1 MPa (4076 psi); coefficient of variation = 0.023.

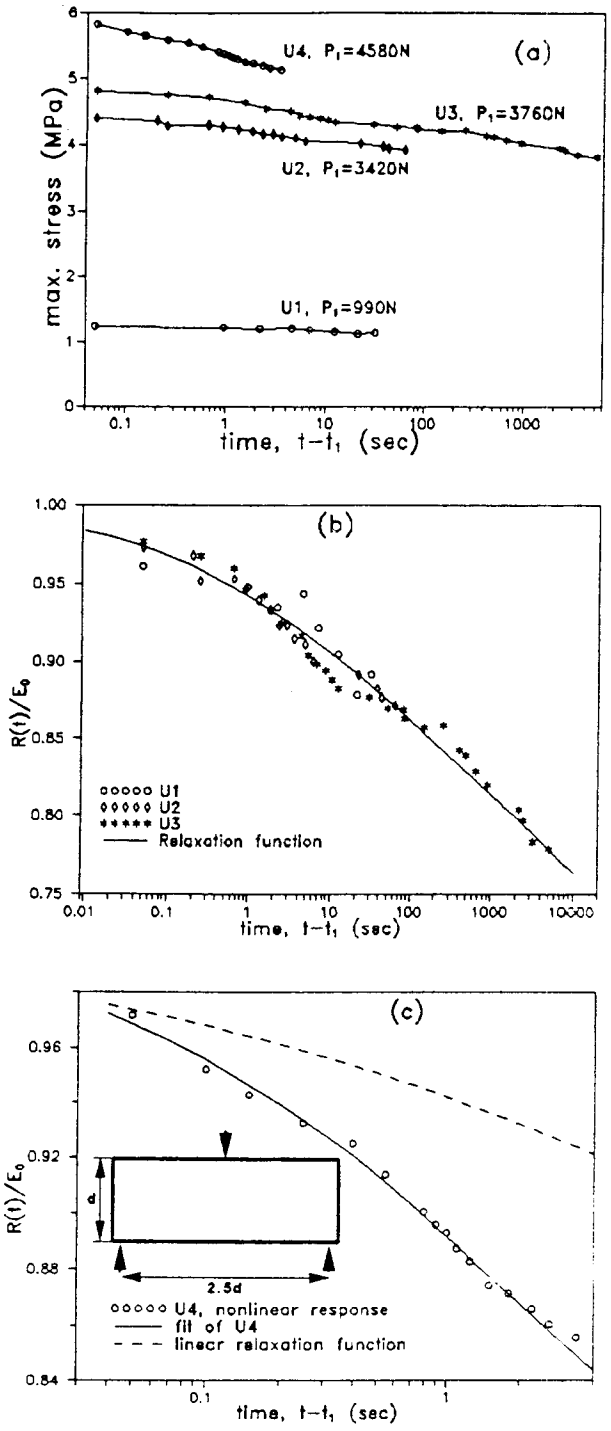

Fig. 9 — Relaxation tests of unnotched beams: (a) experimental data, (b) relaxation in linear range, and (c) relaxation in nonlinear range

nonlinear creep range where relative creep is stress-dependent. This is the case if an initial maximum bending stress greater than about 60 percent of the strength is imposed. At lower stresses, the relative creep or relaxation is generally linear, i.e., independent of stress.[27]

CREEP PROPERTIES OF CONCRETE

To interpret the relaxation tests of fracture specimens (discussed later), one must first know the relaxation properties of the concrete outside the process zone, characterized by the relaxation function $R(t,t_1)$, where t = current time and t_1 = age at the start of relaxation. The appropriate expression for $R(t,t_1)$ may be deduced from the compliance function $J(t,t_1)$ for creep. The log-double power law[37] for the creep of concrete gives a good approximation: $R(t,t_1) \cong 1/J(t,t_1)$. Here, $J(t,t_1) = E_0^{-1}(1 + \xi)$ and $\xi = a\ ln[1 + b(t - t_1)^n]$, where E_0, a, b, and n = empirical constants. For relatively short-term relaxation (hours rather than years), ξ is small. Then $1/(1 + \xi) \cong 1 - \xi$. This leads to the approximation

$$\frac{\sigma}{\epsilon_0} = R(t, t_1) = E_0\{1 - a\ ln[1 + b(t - t_1)^n]\} \quad (8)$$

where σ = current bending stress, ϵ_0 = strain during relaxation, and E_0 = instantaneous modulus, i.e., modulus for extremely fast load application. This modulus is typically 1.5 to 2 times larger than the conventional elastic modulus E that corresponds to the initial slope of the stress-strain diagram in a typical static test (the reason is that loads of several minutes duration suffice to produce considerable creep).[38]

The relaxation tests that were in the linear range (U1, U2, U3) were fitted with Eq. (8) using nonlinear optimization with the Marquardt-Levenberg algorithm. The parameters obtained were n = 0.36, a = 0.063, and b = 1.52, with t and t_1 in sec. Fig. 9(b) shows the fit and the data sets. The coefficient of variation was ω = 0.053. The average E_0 was 54,000 MPa (7.83 × 10^6 psi), with coefficient of variation 0.1.

For the nonlinear (high-stress) range of relaxation, the values for Specimen U4 [see Fig. 9(c)] were E_0 = 56,000 MPa (8.12 × 10^6 psi), n = 0.69, a = 0.056, and b = 5.91, with ω = 0.019.

RELAXATION TESTS OF FRACTURE SPECIMENS

To gain further insight into the rate effect, time-dependent tests of a different type are desirable. Creep tests are not feasible in the post-peak stage, since the load cannot be held constant. But load relaxation tests are possible, as the deformation (e.g., CMOD in fracture tests) can be held constant. In this study, two series of relaxation tests were conducted on 3PB fracture specimens (Fig. 1) with d = 76 mm (3 in.). In the first series, the beams were loaded at several CMOD rates into the post-peak stage and relaxation was initiated at about 80 percent of the peak load. In the second series (described later), the same CMOD rate was used for all specimens but relaxation was initiated at different loads.

The beams NA1, NA2, NA3, and NA4 (first series) were loaded at constant CMOD rates [see Fig. 10(a) and Table 5, where P_{max} = peak load), until a load P_1 ($\cong 0.8\ P_{max}$) was reached at time t_1. Subsequently, the CMOD was held constant, and the relaxation of load with elapsed time $t - t_1$ was then recorded. The measured curves of load versus elapsed time are shown in Fig. 10(b). It is obvious that not only the maximum

Table 5 — Details of fracture relaxation tests

Specimen	f'_c, MPa	Age, days	CMOD rate,* mm/sec	P_{max}, N	P_1, N
NA1†	33.7	136	8.5×10^{-3}	3690	3370
NA2†		138	8.5×10^{-3}	3670	3050
NA3†		140	8.5×10^{-4}	3290	2530
NA4†		136	8.5×10^{-5}	2710	2250
NB1†	35.2	38	8.5×10^{-3}	3600	3460
NB2†		37		3870	3680
NB3†		50		3810	2130
NB4†		36		3880	1620
NB5‡		51		3430	3430
NB6§		43		—	2390

*Loading rate before relaxation.
†Relaxation initiated in post-peak stage.
‡Relaxation initiated near peak load.
§Relaxation initiated in prepeak stage.
1 MPa = 145.04 psi.

load but also the relaxation is strongly influenced by the loading rate. Initially, the rate of relaxation is higher for specimens that are loaded faster, but the final slopes are almost the same regardless of the rate of initial loading. This was expected for two reasons: 1) according to the hereditary aspect of linear viscoelasticity, the initial stress relaxation is higher for a specimen loaded faster, as indicated by the superposition integral over the past stress history;[27] and 2) when a specimen is loaded at a higher rate, there is more damage (larger fracture process zone), and higher stresses near the crack tip. After some time, the delayed linear viscoelastic effect of the early loading history becomes negligible, and the stresses in the process zone relax to about the same values. Therefore, the relaxation rate eventually becomes the same for all specimens.

For the load relaxation after time t_1, the expression for linear stress relaxation [Eq. (8)] may be used as

$$P(t)/P_1 = 1 - A\ 1n[1 + B(t - t_1)^N] \qquad (9)$$

but the values of the empirical parameters A, B, and N are expected to differ from a, b, and n. For short times $t - t_1$, this equation can be approximated by $P(t)/P_1 = 1 - AB(t-t_1)^N$, and for long times $t - t_1$, by $P(t)/P_1 = (1 - A\ 1nB) - AN\,1\,n(t-t_1)$. Thus, the product AN represents the final slope of the plot $P(t)/P_1$ versus $1\,n(t-t_1)$, and Parameter B engenders a horizontal shift representing acceleration or retardation.

The data of Specimens NA1, NA2, NA3, and NA4 were fitted with Eq. (9) by optimizing $P(t)/P_1$ [see Fig. 10(c)]. In the fitting, the final slope (Parameters A and N) was taken to be the same for all four specimens, while B varied. The trends are modeled reasonably well. The parameters and the coefficient of variation ω of the fit are listed in Table 6.

The effects of load and loading stage on relaxation were investigated in the second test series. Six specimens were tested: four in the post-peak stage, one near the peak, and one in the prepeak stage [see Table 5 and Fig. 11(a) and (b)]. (Note that Specimen NB5, loaded until the estimated peak was reached, could lie in either the prepeak or post-peak stage.) The CMOD rate before relaxation was 8.5×10^{-3} mm/s for all these specimens. The load relaxation plots are shown in Fig.

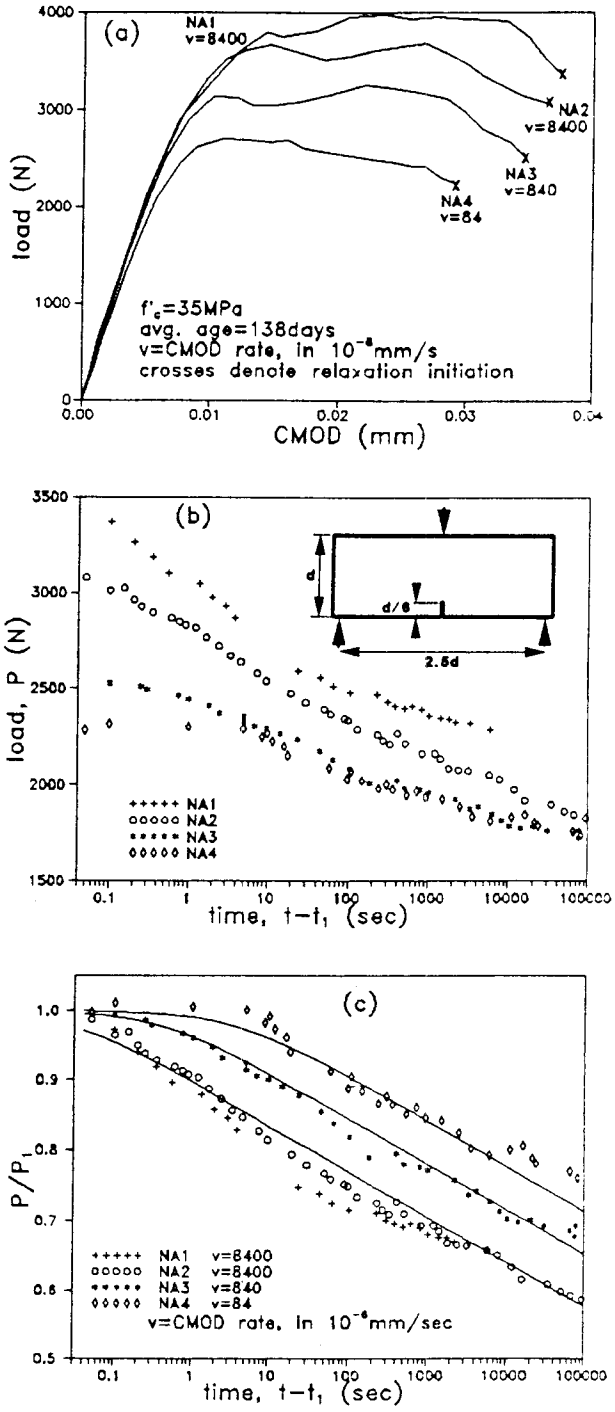

Fig. 10 — Relaxation tests of fracture specimens in post-peak state for various CMOD rates: (a) load-CMOD curves before relaxation, (b) load relaxation, and (c) fits of data with model

Table 6 — Parameters of relaxation function

Specimen	A	B	N	ω
NA1, NA2	0.032	23.8	0.875	0.020
NA3	0.032	2.25	0.875	
NA4	0.032	0.335	0.875	
NB1, NB2, NB3, NB4	0.036	23.8	0.864	0.032
NB5	0.034	23.8	0.770	0.018
NB6	0.034	9.42	0.683	0.008

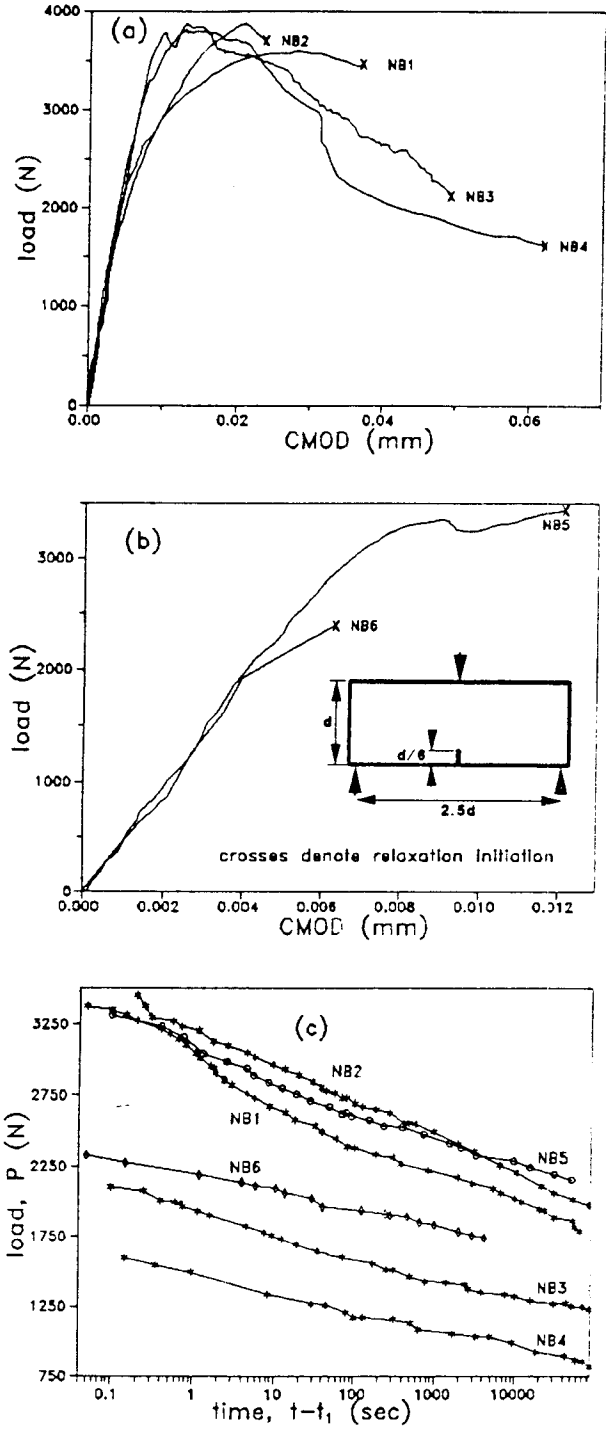

Fig. 11 — Relaxation tests of fracture specimens at same CMOD rates but different load ratios: (a) load-CMOD curves before relaxation of specimens loaded beyond the peak, (b) load-CMOD curves before relaxation of specimens at and before peak, (c) load relaxation

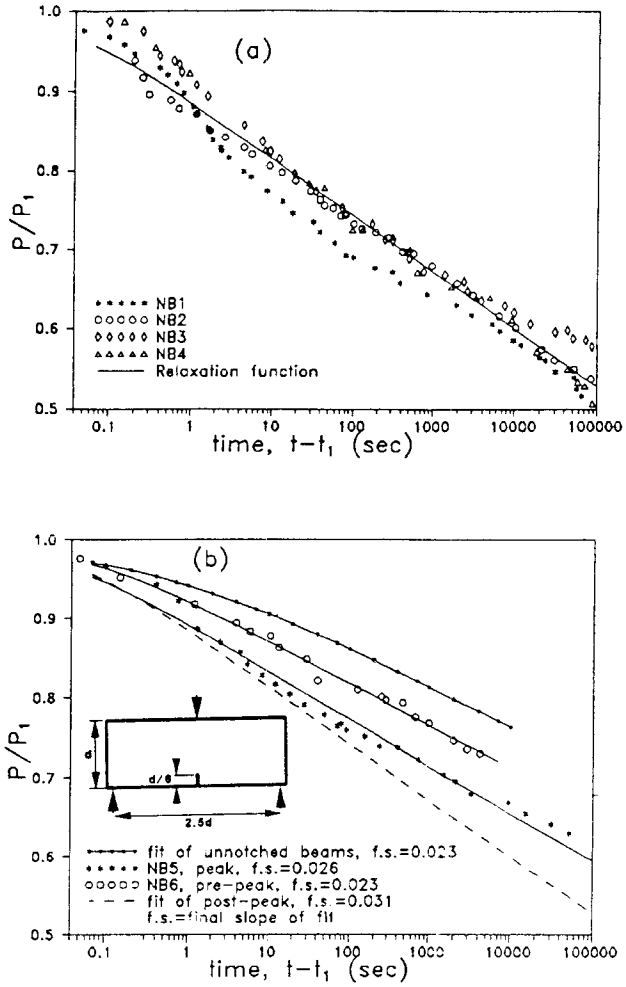

Fig. 12 — Fits of specimen relaxation with model: (a) response in post-peak stage, and (b) response at different levels of loading compared with unnotched beams

11(c). One interesting result is that the relaxation in the post-peak state appears unaffected by the load P_1 at which the relaxation begins. In other words, irrespective of where relaxation is initiated after the peak, $P(t)/P_1$ is the same.

The data of Specimens NB1, NB2, NB3, and NB4 (post-peak state) were fitted by Eq. (9) with $B = 23.8$, which was the value obtained for the same CMOD rate when Specimens NA1 and NA2 of the first series were fitted [see Tables 5 and 6, and Fig. 12(a)]. The values obtained for N and A are about the same. The data for relaxation near the peak (NB5) and in the prepeak stage (NB6) were also fitted with Eq. (9). For NB5, due to lack of sufficient data, the value $B = 23.8$ (from post-peak fits) was used. The fits are shown in Fig. 12(b), and the parameters in Table 6. For comparison, the fits of the post-peak data [from Fig. 12(a)] and linear relaxation [unnotched beams from Fig. 9(b)] are also shown.

It is important to note that the relative relaxation in the post-peak regime is significantly greater than linear relative relaxation. The difference between these two relaxations must be entirely attributed to time-dependent behavior of the fracture process zone.

The responses at the peak and in the prepeak stage lie between the post-peak and linear responses. The basic finding is that, in the time range of these tests, relaxation coincides with the linear behavior at low initial loads before the peak, later increases as the initial load increases towards the peak and, most importantly, remains constant through the post-peak range. Also,

there seems to be an acceleration in relaxation with increase of initial load before the peak. This is similar to the acceleration due to increase in the loading rate [see Fig. 10(c)], and can be explained similarly. To understand these results, it can be hypothesized that the process zone size increases monotonically with the load in the prepeak range, but propagates without much change in size during the post-peak stage (until it gets too close to the end of the ligament); see References 5, 6, 30, and also 39. The delayed linear viscoelastic effect in the post-peak range does not change if the initial loading rate remains the same. Thus, a dependence of the load relaxation on the damage or process zone size can explain the observed trends.

It appears that when a large crack is present in a concrete specimen or structure, the effects of creep are much more significant than without such a crack. Vice versa, creep decreases the load-carrying capacity of the cracked structure considerably. Thus, the interaction of creep and fracture is very important for calculating the response, and eventually for determining the serviceability of structures. This is crucial because long-term creep deformations in concrete structures are considerably larger than the instantaneous deformations.

CONCLUSIONS

1. The size effect law proposed by Bažant agrees with concrete fracture test results over a wide range of loading rates, with times to peak ranging from 1 s to 250,000 s.

2. The test results also show that a decrease of loading rate in this range causes a shift to the right in the size effect plot, i.e., toward higher brittleness and linear elastic fracture mechanics behavior.

3. The fracture toughness, effective length of the fracture process zone, and effective critical crack-tip opening decrease with an increase in the time to peak load. These material fracture parameters were obtained through the size effect method by quasi-elastic analysis based on the effective modulus for creep. An explanation for the decrease in process zone size might be the relaxation of high stresses in the fracture process zone.

4. For the fracture specimen type and time range studied, there is strong load relaxation at constant CMOD in the post-peak regime. The post-peak relaxation is about 1.7 times stronger than that of unnotched specimens. This significant difference may be attributed to 1) additional creep in the fracture process zone, and 2) time-dependent crack growth.

5. The load-relaxation curves tend to a straight line in the logarithm of the elapsed time.

6. There is a strong interaction between fracture and creep in concrete, which is very important for both failure and serviceability analyses of structures. Analysis of long-term fracture propagation in concrete must take this interaction into account.

ACKNOWLEDGMENTS

This work was partially supported by the NSF Center for Advanced Cement-Based Materials (Grant DMR-8808432), and by AFOSR Contract 49620-87-C-0030DEF with Northwestern University. The help of undergraduate research assistants D. Klein and D. Coe in specimen preparation and analysis of data is gratefully acknowledged.

REFERENCES

1. Shah, S. P., and Chandra, S., "Fracture of Concrete Subjected to Cyclic and Sustained Loading," ACI JOURNAL, *Proceedings*, V. 67, No. 10, Oct. 1970, pp. 816-825.

2. Wittmann, F. H., and Zaitsev, Ju., "Behavior of Hardened Cement Paste and Concrete under High Sustained Load," *Mechanical Behavior of Materials*, Proceedings of 1971 International Conference, V. 4, Society of Materials Science, Japan, 1972, pp. 84-95.

3. Liu, Z.-G.; Swartz, S. E.; Hu, K. K.; and Kan, Y.-C., "Time-Dependent Response and Fracture of Plain Concrete Beams," *Fracture of Concrete and Rock: Recent Developments* (International Conference, Cardiff, UK), S. P. Shah, S. E. Swartz, and B. Barr, eds., Elsevier Applied Science, London, 1989, pp. 577-586.

4. Mindess, S., and Shah, S. P., eds., *Cement-Based Composites: Strain Rate Effects on Fracture*, Materials Research Society Symposium Proceedings, V. 64, 1986, 270 pp.

5. Bažant, Z. P., and Gettu, R., "Determination of Nonlinear Fracture Characteristics and Time Dependence from Size Effect," *Fracture of Concrete and Rock: Recent Developments* (International Conference, Cardiff, UK), S. P. Shah, S. E. Swartz, and B. Barr, eds., Elsevier Applied Science, London, 1989, pp. 549-565.

6. Bažant, Z. P., and Gettu, R., "Size Effect in Concrete and Influence of Loading Rate," *Serviceability and Durability of Construction Materials* (Proceedings, First Materials Engineering Conference, Denver), B. A. Suprenant, ed., ASCE, New York, 1990, pp. 1113-1123.

7. Rüsch, H., "Researches toward a General Flexural Theory for Structural Concrete," ACI JOURNAL, *Proceedings* V. 57, July 1960, pp. 1-28.

8. Reinhardt, H. W., "Strain Rate Effects on the Tensile Strength of Concrete as Predicted by Thermodynamic and Fracture Mechanics Models," *Cement-Based Composites: Strain Rate Effects on Fracture*, Materials Research Society Symposium Proceedings, V. 64, S. Mindess and S. P. Shah, eds., 1986, pp. 1-14.

9. Harsh, S.; Shen, Z.; and Darwin, D., "Strain-Rate Sensitive Behavior of Cement Paste and Mortar in Compression," *ACI Materials Journal*, V. 87, No. 5, Sept.-Oct. 1990, pp. 508-516.

10. Hughes, B. P., and Watson, A. J., "Compressive Strength and Ultimate Strain of Concrete under Impact Loading," *Magazine of Concrete Research*, V. 30, No. 105, Dec. 1978, pp. 189-199.

11. Suresh, S.; Nakamura, T.; Yeshurun, Y.; Yang, K.-H.; and Duffy, J., "Tensile Fracture Toughness of Ceramic Materials: Effects of Dynamic Loading and Elevated Temperatures," *Journal of the American Ceramic Society*, V. 73, No. 8, 1990, pp. 2457-2466.

12. Wittmann, F. H., "Influence of Time on Crack Formation and Failure of Concrete," *Application of Fracture Mechanics to Cementitious Composites*, S. P. Shah, ed., Martinus Nijhoff Publishers, Dordrecht, The Netherlands, 1985, pp. 593-616.

13. Lajtai, E. Z.; Schmidtke, R. H.; and Bielus, L. P., "Effect of Water on the Time-dependent Deformation and Fracture of a Granite," *International Journal of Rock Mechanics and Mineral Science*, V. 24, No. 4, 1987, pp. 247-255.

14. Bažant, Z. P., and Prat, P. C., "Effect of Temperature and Humidity on Fracture Energy of Concrete," *ACI Materials Journal*, V. 87, No. 4, July-Aug. 1988, pp. 262-271.

15. Rossi, P., and Boulay, C., "Influence of Free Water in Concrete on the Cracking Process," *Magazine of Concrete Research*, V. 42, No. 152, 1990, pp. 143-146.

16. Darwin, D., and Attiogbe, E. K., "Effects of Loading Rate on Cracking of Cement Paste in Compression," *Cement-Based Composites: Strain Rate Effects on Fracture*, Materials Research Society Symposium Proceedings, V. 64, S. Mindess and S. P. Shah, eds., 1986, pp. 167-180.

17. Chong, K. P., and Boresi, A. P., "Strain Rate Dependent Mechanical Properties of New Albany Reference Shale," *International Journal of Rock Mechanics and Mineral Science*, V. 27, No. 3, 1990,

pp. 199-205.

18. Reinhardt, H. W., "Tensile Fracture of Concrete at High Rates of Loading," *Application of Fracture Mechanics to Cementitious Composites,* S. P. Shah, ed., Martinus Nijhoff Publishers, Dordrecht, The Netherlands, 1985, pp. 559-592.

19. Ross, C. A., and Kuennen, S. T., "Fracture of Concrete at High Strain-Rates," *Fracture of Concrete and Rock: Recent Developments,* S. P. Shah, S. E. Swartz, and B. Barr, eds., Elsevier Applied Science, London, 1989, pp. 152-161.

20. Zielinski, A. J., "Fracture of Concrete and Mortar under Uniaxial Impact Tensile Loading," PhD thesis, Delft University, The Netherlands, 1982.

21. John, R.; Shah, S. P.; and Jenq, Y.-S., "Fracture Mechanics Model to Predict the Rate Sensitivity of Mode I Fracture of Concrete," *Cement and Concrete Research,* V. 17, 1987, pp. 249-262.

22. Wittmann, F. H.; Roelfstra, P. E.; Mihashi, H.; Huang, Y.-Y.; Zhang, X.-H.; and Nomura, N., "Influence of Age of Loading, Water-Cement Ratio and Rate of Loading on Fracture Energy of Concrete," *Materials and Structures, Research and Testing* (RILEM, Paris), V. 20, 1987, pp. 103-110.

23. Bažant, Z. P., "Size Effect in Blunt Fracture: Concrete, Rock, Metal," *Journal of Engineering Mechanics,* ASCE, V. 110, No. 4, 1984, pp. 518-535.

24. Bažant, Z. P., and Pfeiffer, P. A., "Determination of Fracture Energy from Size Effect and Brittleness Number," *ACI Materials Journal,* V. 84, No. 6, Nov.-Dec., 1987, pp. 463-480.

25. Bažant, Z. P., and Kazemi, M. T., "Determination of Fracture Energy, Process Zone Length and Brittleness Number from Size Effect, with Application to Rock and Concrete," *International Journal of Fracture Mechanics,* V. 44, 1990, pp. 111-131.

26. Gettu, R.; Bažant, Z. P.; and Karr, M. E., "Fracture Properties and Brittleness of High-Strength Concrete," *ACI Materials Journal,* V. 87, No. 6, Nov.-Dec. 1990, pp. 608-618.

27. RILEM TC69, Chapter 2, *Mathematical Modeling of Creep and Shrinkage of Concrete,* Z. P. Bažant, ed., John Wiley, Chichester and New York, 1988, pp. 99-216.

28. Wong, W., and Miller, R. A., "Mixed Mode Fracture at Early Ages," *Micromechanics of Failure of Quasi-Brittle Materials* (Proceedings of International Conference, Albuquerque), S. P. Shah, S. E. Swartz, and M. L. Wang, eds., Elsevier Applied Science, London, 1990, pp. 166-175.

29. Bažant, Z. P., "Fracture Energy of Heterogeneous Materials and Similitude," *Fracture of Concrete and Rock* (SEM-RILEM International Conference), S. P. Shah and S. E. Swartz, eds., Springer-Verlag, New York, 1989, pp. 229-241.

30. Bažant, Z. P.; Gettu R.; and Kazemi, M. T., "Identification of Nonlinear Fracture Properties from Size Effect Tests and Structural Analysis Based on Geometry-Dependent R-Curves," *International Journal of Rock Mechanics and Mineral Science,* V. 28, No. 1, 1991, pp. 43-51; Corrigenda, V. 28, No. 2/3, 1991, p. 233.

31. RILEM TC89 Draft Recommendation, "Size-Effect Method for Determining Fracture Energy and Process Zone Size," *Materials and Structures, Research and Testing* (RILEM, Paris), V. 23, 1990, pp. 461-465.

32. Tada, H.; Paris, P. C.; and Irwin, G. R., *Stress Analysis of Cracks Handbook,* 2nd ed., Paris Products, St. Louis, 1985.

33. Bažant, Z. P., and Panula, L., "Practical Prediction of Time-Dependent Deformations of Concrete, Part I: Shrinkage and Part II: Basic Creep," *Materials and Structures, Research and Testing* (RILEM, Paris), V. 11, No. 65, 1978, pp. 307-328.

34. Bažant, Z. P., and Oh, B. H., "Crack Band Theory for Fracture of Concrete," *Materials and Structures, Research and Testing* (RILEM, Paris), V. 16, No. 93, 1983, pp. 155-177.

35. Mindess, S., "Rate of Loading Effects on the Fracture of Cementitious Materials," *Application of Fracture Mechanics to Cementitious Composites,* S. P. Shah, ed., Martinus Nijhoff Publishers, Dordrecht, The Netherlands, 1985, pp. 617-638.

36. Oh, B.-H., and Chung, C.-H., "Fracture Energy of Concrete under Static and Dynamic Loading," Preprints of the *Proceedings,* International Workshop on Fracture Toughness and Fracture Energy — Test Methods for Concrete and Rock, Sendai, Japan, 1988, pp. 360-372.

37. Bažant, Z. P., and Chern, J.-C., "Double-Power Logarithmic Law for Concrete Creep," *Cement and Concrete Research,* V. 14, 1984, pp. 793-806.

38. Bažant, Z. P., ed., *Mathematical Modeling of Creep and Shrinkage of Concrete,* J. Wiley, Chichester and New York, 1988, 459 pp.

39. Liu, Z.-G.; Swartz, S. E.; and Hu, K. K. "Two-Dimensional Finite Element Modeling of Crack Growth in Concrete Using Three-Dimensional Damage Data," *Micromechanics of Failure of Quasi-Brittle Materials* (Proceedings of International Conference, Albuquerque), S. P. Shah, S. E. Swartz, and M. L. Wang, eds., Elsevier Applied Science, London, 1990, pp. 176-187.